Science and Technology Indonesia
e-ISSN:2580-4391 p-ISSN:2580-4405
Vol. 9, No. 4, October 2024

Research Paper

Characteristics and Dosimetric Properties of Tissue-Equivalent Thermoluminescent Glass Detector Based on Al-Li-Zn, Borate Oxide Dope Dy^{3+}

Godwin Irinam Efenji[1,2*], Iskandar Shahrim Bin Mustafa[1], Nur Nabihah Yusof[1], Rabba James Anthony[2], Ferdinand Ayim Kamgba[6], Ushie P. O.[6], Thair Hussein Khazaalah[1], Munirah Jamil[8], Muhammad Fadhirul Izwan[1], Umar Sa'ad Aliyu[3], Nabasu Seth Ezra[1], Aduragbemi Olaoluwa Oke[7], Hayder Salah Naeem[1], Alhassan Muhammad[1,4], Ali S. A. Idriss [1,5]

[1]*School of Physics, Universiti Sains Malaysia, Penang, 11800, Malaysia*
[2]*Department of Physics, Federal University Lokoja, Kogi State, P.M.B. 1154, Nigeria*
[3]*Department of Physics, Federal University Lafia, P.M.B. 146, Nigeria*
[4]*Department of Physics, Federal Federal University, Dutsin-Ma., Dutsin-ma, Katsina state, P.M.B. 5001, Nigeria*
[5]*Higher Institute of Science and Technology Tamzawa, Al Shati', 218-733, Libya*
[6]*Cross River University of Technology, Calabar, P.M.B. 1123, Nigeria*
[7]*Department of Physics, Federal University Oye-Ekiti, P.M.B. 373, Nigeria*
[8]*Department of Chemistry and Materials Engineering, Faculty of Chemistry, Materials and Bioengineering Kansai University 3-3-35 Yamate-cho, Suita, Osaka, 564-8680, Japan*
*__Corresponding author__: godwin.efenji@fulokoja.edu.ng

Abstract
The functionality and dosimetric properties of a tissue-equivalent thermoluminescent glass detector doped with Dy^{3+} were investigated in this work. This work investigated an Aluminium-Lithium-Zinc borate oxide matrix using the melting-quench method. X-ray diffraction confirms the glass sample is amorphous. Dysprosium ions doping raises the glass's tissue equivalent effective atomic number ($Z_{eff.}$), improving its ability to absorb radiation and its sensitivity, with reproducibility almost at the tolerable limit. The glass detector also reduces the fading rate and signal loss over time. The minimum detectable dose values were 53.04 mGy and 45.1 mGy for the un-doped and 1.5 mol Dy^{3+} doped Al-Li-Zn borate glasses, respectively. A bright peak was seen in photoluminescence spectra at 348 nm (yellow), 529 nm (green), and 625 nm (orange hue). These correspond to the Dy^{3+} transitions at $^4H15/2 \rightarrow {}^6P7/2$, $^4F9/2 \rightarrow {}^6H15/2$, $^4F9/2 \rightarrow {}^6H15/2$, and $^4F9/2 \rightarrow {}^6H13/2$, respectively. There was a noticeable drop in Tg from 257°C in the undoped sample to 101°C in the doped sample, Tm from 862°C to 815°C, and Tc from 756°C to 444°C in the doped sample. These results may indicate a lower temperature at which the material transitions from a solid to a liquid state and a lower crystallisation threshold. The frequency component and energy of activation of the 1.5 mol Dy^{3+} doped Aluminium-Lithium-Zinc borate are 2.1×10 27 s^{-1} and 1.03 eV, respectively. The 1.5 Dy^{3+} doped Aluminium-Lithium-Zinc borate glasses exhibit promising dosimetric properties of the tissue-equivalent thermoluminescent glass detector, indicating its potential for accurate and consistent radiation dosimetry in various applications.

Keywords
Borate Oxide Dope, Tissue-Equivalent Thermoluminescence Dosimeter Glass Detector, Glass Detector, Thermoluminescence Emission

Received: 8 April 2024, Accepted: 18 July 2024
https://doi.org/10.26554/sti.2024.9.4.965-980

1. INTRODUCTION

Radiation dosimetry is essential in many domains, such as industrial processes, radiation therapy, environmental monitoring, and medical diagnostics (Ullah et al., 2024). Ensuring worker safety, maximising treatment efficacy, and adhering to regulatory requirements all depend on accurate and trustworthy ionising radiation measurement (Aljewaw et al., 2023; El-Faramawy et al., 2021). Because of its tissue-equivalent qualities, high sensitivity, and broad dynamic range, thermoluminescent dosimeters (TLDs) have become valuable instruments among the various dosimetry techniques available (Khandaker et al., 2024; White et al., 2024). With the dynamic needs of radiation dosimetry applications, significant research efforts focused on developing innovative TLD materials with improved properties in recent years (Godwin et al., 2023).

Tissue-equivalent thermoluminescent glass detectors based on Al-Li-Zn borate oxide doped with Dy^{3+} ions are one viable possibility in this endeavour. Compared to typical TLD

materials, these glass detectors have higher tissue equivalency, increased sensitivity, and stability in various environmental conditions (Ullah et al., 2024). When rare-earth dopants like Dy^{3+} are added to the glass matrix, luminescent centres are created that can effectively absorb and store energy from ionising radiation; this allows for precise dosage assessments to be made when the material is heated later (Bootjomchai and Laopaiboon, 2014; Pawar et al., 2017).

This study's primary goal is to thoroughly examine the features and dosimetric attributes of tissue-equivalent thermoluminescent glass detectors made of Dy^{3+} doped Al-Li-Zn borate oxide. This study attempts to clarify the material's suitability for various radiation dosimetry applications by methodically investigating its structural, optical, thermal, and luminescent properties (Godwin et al., 2023; Stanković Petrović et al., 2021).

A multidisciplinary strategy that includes a range of characterisation approaches to examine various facets of the behaviour of the glass detector will be used to accomplish this goal. We use X-ray diffraction (XRD) analysis to determine the glass matrix's crystalline phases and structural makeup (Pal et al., 2011). UV-vis spectroscopy optical characterisation will allow the glass's absorption and emission properties to be examined, especially with Dy^{3+} ions. Thermogravimetric analysis (TGA) in conjunction with differential thermal analysis (DTA) will evaluate the glass's behaviour and thermal stability at various temperatures, offering information on how the material will react to radiation exposure (Bradley et al., 2020; Sani et al., 2020).

Moreover, the molecular structure and bonding topologies inside the glass matrix were examined using Fourier-transform infrared (FTIR) spectroscopy, which will provide essential details on the material's chemical makeup and any interactions with ionising radiation. Using a TLD reader, the thermoluminescence characteristics of the glass detector will be carefully examined to determine whether it is suitable for precise dosage measurement. This analysis will include background noise measurements, glow curve deconvolution, and trap parameter estimation (Prabhu et al., 2021; Aljewaw et al., 2020).

This study comprehensively examines tissue-equivalent thermoluminescent glass detectors' characteristics and dosimetric performances based on Al-Li-Zn borate oxide doped with Dy^{3+} ions to develop radiation dosimetry approaches. With the help of this research, novel dosimetry solutions with enhanced performance, dependability, and adaptability may be developed to meet the changing requirements of diverse fields that depend on precise radiation dose assessments.

2. EXPERIMENTAL SECTION

2.1 Chemicals Elements

The following chemicals were purchased from reliable suppliers and were of analytical quality: 'Sigma Aldrich Germany,' which had 99.99% purity. These include Boron oxide (B_2O_3), Aluminium oxide (Al_2O_3), Lithium oxide (Li_2O), Zinc oxide (ZnO) and Dysprosium oxide (Dy_2O_3)

2.2 Instrumentation

Stainless steel mould, electric weighing balance, platinum crucible, mixing mortar, TLD (Harshaw TLD 3500), XRD (PANalytical X'Pert PRO MRD PW3040 X-ray diffractometer), FTIR (PerkinElmer Model System 2000, USA), UV-Vis-NIR spectroscopy (Agilent Cary 5000), DTA (Thermogravimetric Analyzer, STA 600), and PL (PerkinElmer LS 55 Fluorescence Spectrometer).

2.3 Glass Fabrication

The glass samples were fabricated by employing a special technique known as melt-quenching. The glass samples were measured and mixed according to the formula in mole percent created by employing the standard melting and quenching technique. The raw ingredients were purchased from Sigma Aldrich Germany with the appropriate amounts of Al_2O_3, Li_2O, B_2O_3, ZnO, and Dy_2O_3. According to the combination formula above, they were weighed and mixed in various mole percentages. These components were hand-mixed and ground for 20 minutes to create a sufficient or uniform mixed powder. After being dissolved in a platinum crucible for uniform melting, the powder combination was heated for three hours at 1300°C in an electrical heating furnace, as seen in Figure 1. The liquid samples were then transferred into a stainless-steel mould and transferred to an annealing machine for gradual annealing at a maximum of 400°C for two hours to relieve internal stresses and cool to ambient temperature. Each sample batch was then polished to ensure smooth surfaces, shaped to a desired shape, and ground-to-powder characterisation.

2.4 Glass Characterisation and Measurement

A Cu Kα (λ = 1.5405 Å) was used for powder X-ray diffraction at 40 kV tube voltage and 40 mA tube current. This was carried out on the Bruker D8 advanced X-ray diffractometer to verify the phase purity of samples. For refinement, the high-quality XRD data was recorded at intervals of 0.2°C throughout a 2θ range, from 10 to 80°C. Thermoluminescence (TL) emission spectra were captured using a fluorescence spectrometer (LS 55 Perkin Elmer, School of Chemical Science Laboratory, USM). The samples were scanned from a wavelength range of 200–900 nm, with 400 nm of light on the material. Utilised The TL reader (HARSHAW TLD 3500, Medical Physics Laboratory, USM) was in conjunction with the samples' thermoluminescence light curves to examine the dose-response (5–45 mGy), reproducibility (24 cycles), and fading (24 days) using the Hamamatsu Photonics R6095 model. The sample was annealed, exposed to radiation, and monitored 24 times to track each shift in the TL integrated signal to evaluate the repeatability. As the practice, the sample was heated to 400°C for ten minutes before naturally cooling to room temperature. It was heated from ambient temperature to 400°C after exposure to 5-45 mGy X-ray to produce a matching TL glow curve. The above method was repeated to determine the TL intensity, and the highest temperature TL band was integrated. Six sets of glass samples, three samples per set, were individ-

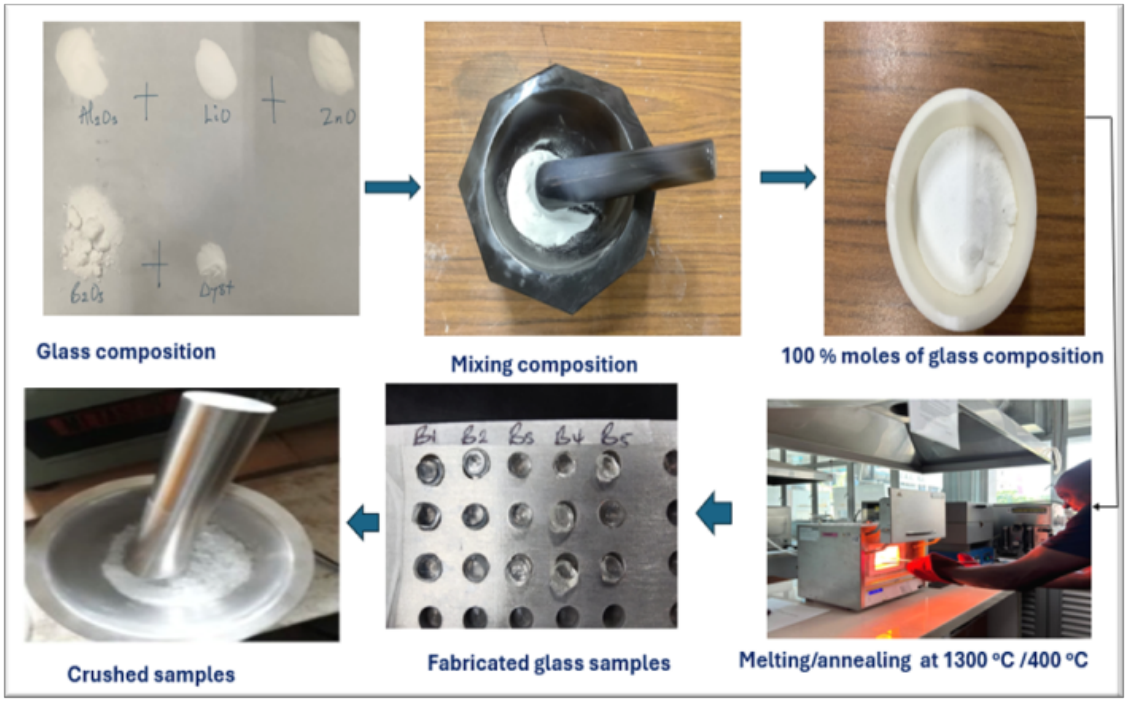

Figure 1. Glass Sample Preparation in Sequential Order

ually exposed to a range of X-ray radiation starting from 5 mGy X-ray before being kept in a lead chamber at room temperature to minimise any potential interference from cosmic rays or outside light to assess the fading property. Every day, a set of samples was removed from the lead chamber, and the TL glow curves were immediately measured. The final set of samples was measured after 24 days. The TL band with the highest temperature was integrated. Each set of samples' average result was computed to assess the fading property and lower the statistical error. All TL curve measurements in this paper had a 10 °C/s rate of heating. The UV-1800 radiation excitation and emission spectra were employed to capture the spectra of absorption in the 200-900 nm VUV-UV range (Medical Physics Laboratory, USM). Differential thermal analysis was carried out in the School of Chemical Sciences Laboratory, USM, using a Thermogravimetric Analyser, STA 600, to assess the thermal stability by gradually raising the samples' temperature from ambient temperature to 1000°C (10 °C/min). The PerkinElmer LS 55 Fluorescence Spectrometer, which gauges the wavelength distribution and intensity of light emitted from the sample when a specific light source activates it, was used to quantify photoluminescence (PL). Both the effective atomic number ($Z_{eff.}$) and the minimum detectable dose (MDD) were calculated theoretically using Equations (12), (14), (15), and (16), respectively.

3. RESULTS AND DISCUSSION

3.1 Glass Formulation

The composition of the manufactured glass (Denoted B), including Dy^{3+} ions, B_2O_3, ZnO, Li_2O, and Al_2O_3, is displayed in Table 1. Al_2O_3 boosts endurance, ZnO enhances optical qualities, B_2O_3 offers a stable matrix, and Li_2O decreases melting temperature and improves stability. Luminous centres are produced using different percentage moles of Dy^{3+} ions, enabling accurate radiation monitoring. Excellent thermoluminescence, structural stability, and radiation sensitivity with an appropriate molar volume and density are the reasons behind the compositional choice of the glass. These characteristics and the glass's unique molecular structure and thermal stability will make it ideal for radiation dosimetry (Satkar et al., 2021; Shafaei and Moradi, 2023).

3.2 X-Ray Diffraction Analysis (XRD)

The X-ray diffraction (XRD) examination technique was employed to investigate the properties of different materials, such as glasses. When examining the Al-Li-Zn doped Dy^{3+} borate glass for radiation dosimetry, XRD analysis is crucial for comprehending and identifying the crystal structure, estimating the proportions of crystalline and non-crystalline phases, calculating lattice parameters, and evaluating the size of crystal particles (El-Adawy et al., 2010; Prabhu et al., 2019). These insightful observations help to clarify the relationship between the structure of the glasses and their intended usage as radiation dosimeters. The XRD spectra of samples varying in the quantity of Dy^{3+} doped Al-Li-Zn glass host throughout the range

Table 1. Al-Li-Zn Borate Glass Composition

Samples of Glass	Compositions of Glass (Mole Fraction%)				
	Dy_2O_3	Li_2O	Al_2O_3	ZnO	B_2O_3
B1 (CS)	0	4.0125	27.3852	21.8572	46.7452
B2	0.4989	3.9925	27.2485	21.7481	46.5119
B3	1.4849	3.9529	26.9785	21.5326	46.0511
B4	2.4553	3.914	26.7128	21.3205	45.5974
B5	3.4106	3.8757	26.4512	21.1117	45.1509
B6	4.816	3.8193	26.0663	20.8045	44.4939

of $10\circ \leq \theta \leq 80$ are displayed in Figure 2. The produced glass sample's XRD pattern lacks identifiable peaks, suggesting that a long-range periodic lattice arrangement that resembles crystals is not present, this demonstrated that the glass was amorphous (Hashim et al., 2017).

3.3 Physical Characteristics

The density of the manufactured glass is one of the primary physical characteristics examined. According to Khazaalah et al. (2022), thickness measures the geometric configuration's structural rigidity and diversity. Equation (1) was used to verify it using the values in Table 2, following Archimedes' principle.

$$\rho = \frac{a}{a - b}\rho_{\text{dist. water}} \tag{1}$$

Here, $\rho_{\text{dist. water}}$ is the distilled water's density, and is the glass sample's weight in the air, and b is the glass sample's weight in the distilled water (Saidu et al., 2018). Equation (2) was used to calculate the Molar volume (V_m) using the values found in Table 2.

$$V_m = \frac{M_{wt}}{\rho} \tag{2}$$

Glass density is related to its structure and composition (see Figure 3). Because they enhance the number of atoms already there without appreciably altering the size of the network, external network ions frequently result in an increase in density. The increase in density caused by the external network ions is more significant, according to Saidu et al. (2014), than the loss in density caused by the network's fracture, expansion, and volume growth. The densities and molar volumes of the glasses are summarised in Table 2.

As shown in Figure 3, the glass composition with the densities of glass samples B3, B4, B5, and B6 increase as the dopant element increases (Dy^{3+}). The dopant's relative atomic mass is 373 times greater than the glass former's (B_{203}) 70.0034, which accounts for the changes. As a result, the glass density increased similarly when heavy atoms were added to the system (Saidu et al., 2014). The B2 glass sample has a lower density, indicating more excellent compatibility between the glass nodes, because the mass of the dopant element is bigger than that of the glass former (Jamil et al., 2023).

Saidu et al. (2014) have established a correlation between compaction of the glass network, the molar volume value and the atomic radius. Put otherwise, they elucidate that the molar volume diminishes as the glass structure compactness increases. A slight rise in molar volume was seen in B2 as the dopant element increased, indicating that the addition of secondary flux (Zn0) did not cause the glass network to constrict.

The permitted molar quantities of B3, B4, and B6 in comparison to B1 indicate that B_{203} functions within the glass network structure as a glass former, incorporating B04 into the glass to increase density and decrease molar volume (Khazaalah et al., 2022). Compared to the other glasses, glass samples B3 and B4 have the densest glass networks since they have the smallest molar volumes.

3.4 Behaviour of the TL Glow Curve

The glow curve is an essential component of TL dosimeters, which provides important information on the signal-fading characteristics, trapping states, and trap depths of the TL material being studied. The various trapping levels and the corresponding light peaks can be identified by evaluating the glow curve's form and location (Aljewaw et al., 2023; Bradley et al., 2020). The graph of the glow curve shows the sample temperatures versus the TL intensity. A perfect light curve and a desired TL material should show one peak between 180 and 250. A phosphor's glow curve is its most important feature; where the glow peaks are located suggests the existence of deep traps At lower temperatures, if any are discovered. Under such circumstances, TL deposited progressively disappears and becomes unusable for extended periods. On the other hand, let us assume that the temperature at which the glow peak is positioned is sufficiently high. Then, at the temperature required for the TL to release, the phosphor emits infrared radiation, which could cause incorrect interpretations of the data.

Figure 4 presents the TL glow curves of Al-Li-Zn borate glass of undoped and doped samples containing different concentrations of Dy^{3+} ions. Table 2 displays the samples' corresponding Dy^{3+} concentrations are 0.0, 0.5, 1.5, 2.5, 3.4, and 4.8 moles. The samples are in batches (B): B1, B2, B3, B4, B5, and B6. The undoped and doped samples were exposed to 5-45 mGy X-ray radiation. The best TL intensity, as shown in Figure 4, was obtained by adding ions to the glass network in batches B2, B3, B4, B5, and B6, as indicated by the TL glow

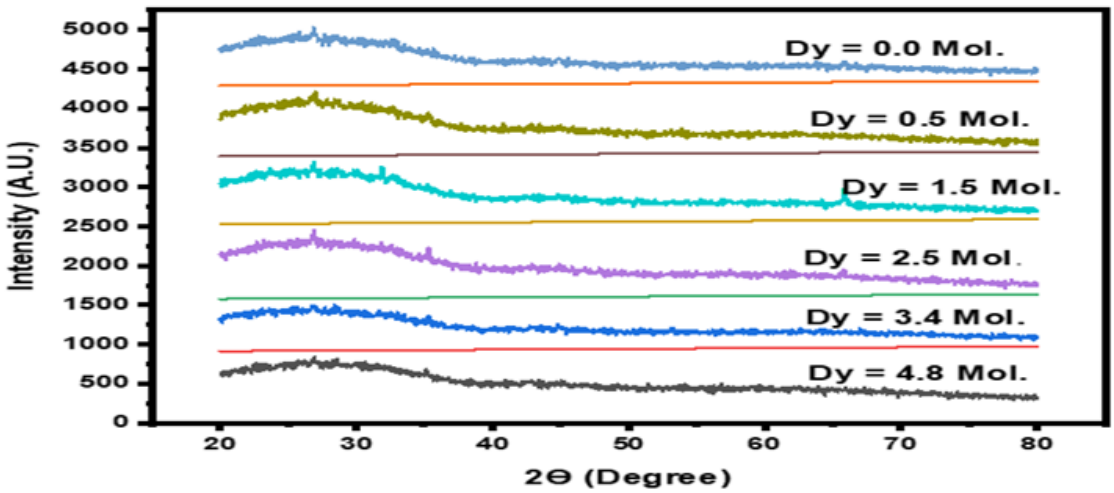

Figure 2. The XRD Spectrum of the Undoped and Dy^{3+} Doped Al-Li-Zn Borate Glass

Table 2. Al-Li-Zn Borate Glass Compositions, Density, and Molar Volume of Undoped and Dy^{3+} Doped Samples

Glass Samples	Glass Compositions (Mole Faction %)					Density (g/cm^3) ± 0.03	Molar Volume (cm^3/mol) ± 0.03
	Dy_2O_3	Li_2O	Al_2O_3	ZnO	B_2O_3		
B1 (CS)	0	4.0125	27.3852	21.8572	46.7452	2.606	29.48
B2	0.4989	3.9925	27.2485	21.7481	46.5119	2.592	29.75
B3	1.4849	3.9529	26.9785	21.5326	46.0511	2.675	29.78
B4	2.4553	3.914	26.7128	21.3205	45.5974	2.695	29.79
B5	3.4106	3.8757	26.4512	21.1117	45.1509	2.745	29.83
B6	4.816	3.8193	26.0663	20.8045	44.4939	2.804	29.89

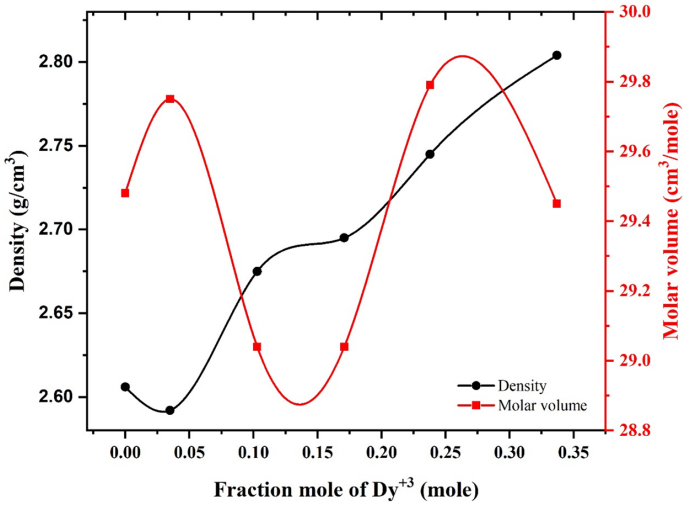

Figure 3. Al-Li-Zn Borate Glass with Undoped and Dy^{3+} Doped Density and Molar Volume and Fractional Mole

curves in (b, c, d, e, and f). However, the most dominant is 1.5 mol. Of Dy^{3+} (c), even at 300°C, the charge collected is still ongoing at 25k compared to the other Dy^{3+} concentrations, (d), (e), and (f), respectively. The intensity is approaching 15k for 4.8 mole at 300°C.

The Dy^{3+} doped Al-Li-Zn borate glasses exhibit uncomplicated glow curves featuring a prominent peak for dosimeters under consideration. As depicted in Figure 4, the glow peak demonstrates a consistent and smooth curve when the Dy^{3+} dopant is introduced, unlike the undoped glass (figure 4a), which lacks Dy^{3+} concentration, as shown in Figure 4. Also, the peak temperature shifted further, supporting this observation. The varying concentration of dopant (Dy^{3+} ions) is likely responsible for this shift in the maximum peak temperature (El-Adawy et al., 2010; Pekpak et al., 2011).

Meanwhile, the displacement of glow peaks towards higher temperatures benefits the thermoluminescence (TL) yield, as glow peaks at more elevated temperatures exhibit improved thermal stability compared to those at lower temperatures (Ullah et al., 2024; White et al., 2024). Notably, Batch B3, the sample with the highest TL intensity, has a glow peak temperature that is within the permissible dosimetry glow peak temperature range. However, burn peaks with temperatures higher than the dosimetry peak limit may harm the residual TL signal (Pekpak et al., 2009; Pekpak et al., 2014).

3.5 Kinetic Parameter Analysis

One must comprehend a material's trapping levels to ascertain its forms, intensities, and peaks of glow. The kinetic factors

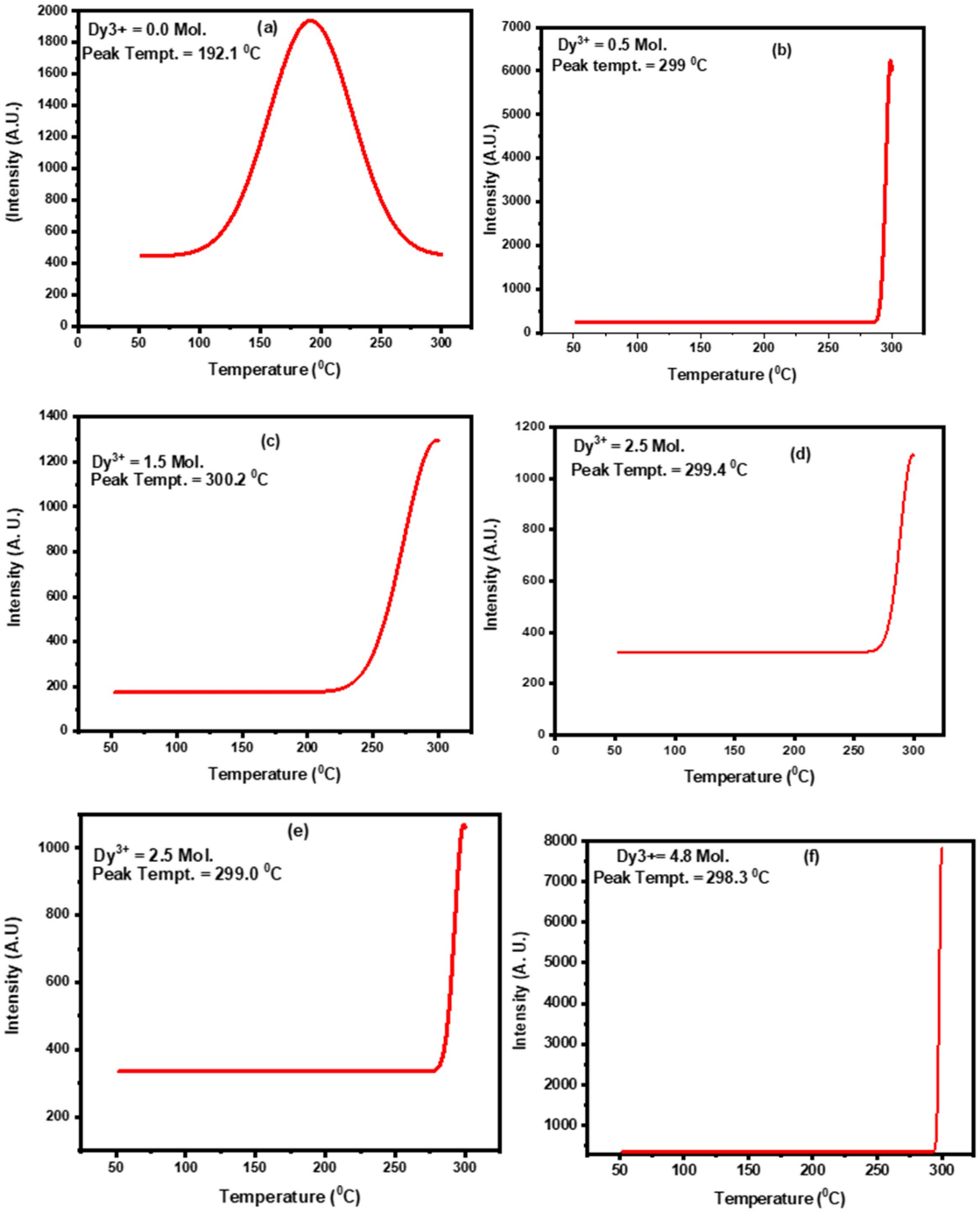

Figure 4. *TL* Glow Curve of (a) Undoped Al-Li-Zn Borate Glasses and (b), (c), (d), (e), and (f) Dy^{3+} Doped Al-Li-Zn Borate Glasses Irradiated by X-Ray Dose 45 mGy

linked to these values could potentially include crucial information about the dosimetric features of the material, particularly the process underlying its TL behaviour (Aljewaw et al., 2023;Wahib et al., 2020).

The frequency factor (s), trap depth, kinetic order (b), and activation energy (E) are the three most important kinetic components. The Peak Shape (PS) technique was used in this investigation to evaluate the activation energy and frequency factor. This technique involves measuring the width of the glow curve and the temperatures corresponding to half of the peak intensity on both the rising and descending sides of the curve (Table 3). Following Chen and Winer's 1970 peak shape

technique (Equation (3)), the geometric component (μ_g) was first approximated using the following relation:

$$\mu_g = \frac{\delta}{\omega} = \frac{T_2 - T_m}{T_2 - T_1} \quad (3)$$

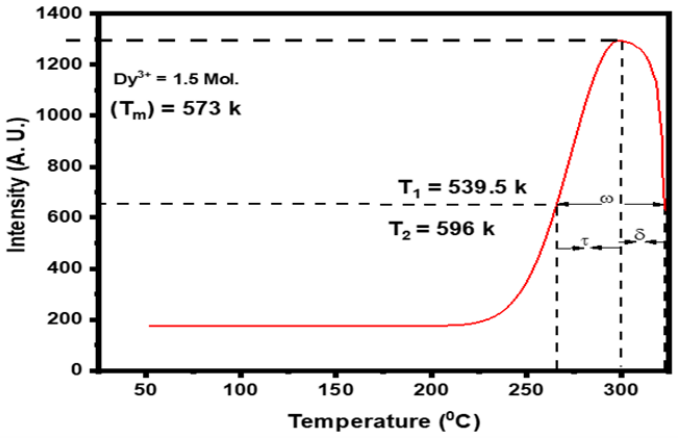

Figure 5. Kinetic Parameters of 1.5 Mol% of Dy^{3+} Doped of Al-Li-Zn Borate Glass Using the Peak Shape Method

where T_2 and T_1 are the temperatures on both sides of T_m, where the high-temperature side corresponds to half of the width. $\omega = T_2 = T_1$ and half-intensity, $\delta = T_2 - T_m$, T_m is the temperature at which the most astounding TL intensity occurs. The kinetic order determines the value of μ_g. It has been observed that the TL material exhibits first- and second-order kinetics, with µg values approximately equal to 0.42 and 0.52, respectively. The frequency factor and activation energy (E) at work can were obtained from the combined operation of Equations (4), (5), (6), (7) and (8) from (Chen and W., 1970) and (Chen and W., 1970):

$$E = C_\alpha \left(\frac{kT_m^2}{\alpha}\right) - b_\alpha (2kT_m) \quad (4)$$

Where k is Boltzmann constant (8.62×10^{-5}) eV K-1 and α can take the place of τ, δ, and ω. The values of C_τ, C_δ, and C_ω are obtained using the following equations.

$$C_\tau = 1.151 + 3.0(\mu - 0.42); b_\tau = 1.58 + 4.2(\mu - 0.42) \quad (5)$$

$$C_\delta = 0.976 + 7.3(\mu - 0.42); b_\delta = 0 \quad (6)$$

$$C_\omega = 2.52 + 10.2(\mu - 0.42); b_\omega = 1 \quad (7)$$

Based on prior values, the factor of frequency (S) is computed using the formula:

$$S = \frac{\beta E}{kT_m^2} exp\left(\frac{E}{kT_m}\right) \quad (8)$$

Where β is the heating rate, and k is the Boltzmann constant (Wahib et al., 2020).

The kinetic properties of Dy^{3+} doped Al-Li-Zn borate glass samples are determined by graphing the temperature versus TL intensity, as illustrated in Figure 5, using the peak shape approach. Using Chen's Equations (3), (4), (5), and (6) correspondingly, TL glow curves at 300°C for the ideal Al-Li-Zn borate glass exposed to a 45 mGy X-ray dosage were calculated for the current experiment as shown in Table 3 (Morsi et al., 2016; Saidu et al., 2015).

After the glow curve's kinetic parameters were ascertained by its use, a geometrical factor (μ_g) of 0.42 was obtained. Based on the geometry and design of the dosimeter system, this value shows how the system reacts to radiation. The dosimeter system may have a unique spatial sensitivity to radiation, which could affect its accuracy in measuring absorbed doses under particular geometrical settings, as indicated by the geometric factor of 0.42 (Chen and W., 1970; Chen, 1969). This number supports earlier findings by showing that recombination follows second-order kinetics (Aljewaw et al., 2023)ig. 5. Table 3 displays the optimal Al-Li-Zn borate glass's frequency factor and activation energy, where the mean values of S and E are 2.1×10^{27} s^{-1} and 1.03 eV, respectively. The kinetics characteristics of the proposed Al-Li-Zn borate glass showed a dose-dependent development that suggested the presence of trap states with stable energy distributions. Higher energy and temperature were required to release the electrons from the deeper-level traps. According to previous research (Saidu et al., 2015; Wahib et al., 2020), these results are consistent.

The number of ionising events per unit when the dosimeter is subjected to radiation is represented by the frequency factor (S). The factor in this instance is $2.1\times10^{2}7$ s^{-1}, a very high figure. This value indicates that the dosimeter can quickly detect many ionising events. The bare minimum energy needed for a radiation event to trigger a discernible reaction in the dosimeter is the activation energy (E). The activation energy in this instance is 1.03 eV. The dosimeter can detect radiation events with a comparatively low energy threshold thanks to its relatively low value. These measurements offer details on the dosimeter's sensitivity and response properties. Its low activation energy and high-frequency factor indicate the dosimeter's high sensitivity to radiation and ability to detect various radiation events. The values are essential for accurately calculating the absorbed dose across multiple radiation environments (Morsi et al., 2016).

3.6 Glass's Sensitivity to X-Rays

The TL sensitivity of a material is a measure of its vulnerability to ionising radiation. It concerns how much light a material can release when heated after exposure to ionising radiation. Selecting a dosimeter of highly thermal shock-sensitive material is better since heated material emits more light, indicating a higher radiation exposure level (Mhareb et al., 2016).

The sensitivity of TL dosimeters is defined as the mass and dosage of the glass material (nCg-1mGy-1) divided by the

Table 3. Al-Li-Zn Borate Glass's Frequency Factor and Activation Energy in 1.5 Mol% Dy^{3+}

	T_m (k)	μ_g	T	Δ	ω	Average
Activation Energy E(eV)	573	0.42	3.1	0.0002	0.0006	1.03
Frequency Factor S(s^{-1})	573	0.42	$6.3 \times 10^2 7$	6.3×10^{-6}	9.6×10^{-4}	$2.1 \times 10^2 7$

strength of the glass samples' TL signal (Prabhu et al., 2021). The following sources were consulted to calculate the value of (*S*):

$$S_{TL} = \frac{TL \text{ intensity } (nC)}{\text{Mass } (g) \times \text{Absorbed Dose } (mGy)} \quad (9)$$

Table 4 shows the total light sensitivity (nC/gmGy) values for Al-Li-Zn borate glasses that are not doped and those doped with 1.5 mol. percent Dy^{3+}. Next, each glass sample's TL sensitivity was ascertained using Equation (9) once the values were acquired by taking the mean of three measurements. It was shown that the optimal Al-Li-Zn borate glass had the highest TL sensitivity, measuring 6527.9 nC/mg Gy. 2731.08 nC/mg Gy was the undoped glass's sensitivity, as shown in Table 4. The 1.5 mol% Dy^{3+} doped glass showed a 3796 nC/mgGy times higher TL sensitivity than the un-doped glass. Therefore, using 1.5 Mol. Dy^{3+} doped, any low radiation doses can be calculated. Based on the comparison with the un-doped glass, the recommended Dy^{3+} doped optimal Al-Li-Zn borate glass appears to have potential as a TL dosimeter material.

3.7 Dose Reproducibility

Reproducibility It is crucial to recognise that a TLD material's repeatability quotient, which indicates its TL efficacy and quality, determines its reusability. The TL signal at a given dosage should hold for several readings. Materials that are repeatedly exposed to readout, annealing, and radiation should not change their physicochemical characteristics. A cluster of dosimeters with comparable features and dosages, or a single dosimeter, can be used to assess the repeatability of thermoluminescence measurement. The repeatability of the system was determined by the SVI or CV percent, which is the mean of the percent standard deviations of each TL detector (De Carvalho et al., 2012). To determine the CV percent caused by the reader, system, and detector, data from annealing, irradiating, and reading multiple dosimeters with identical doses should not be more than ≤7.5 percent (Aydas et al., 2016). According to De Carvalho et al. (2012), the detector's CV percent is expressed using the following formula:

$$DVI = \sqrt{(SVI)^2 - (RVI)^2} \quad (10)$$

The reader variability index is called RVI, and the percent standard deviations of the mean values of each cycle of readings is calculated as CV percent = STD/mean × 100. On the other hand, SVI, also known as CV percent = STD/X × 100, is the average of the percent standard deviations for every specimen in the TL detector. The index of detector variability is DVI (Aljewaw et al., 2023).

The matching SVI and RVI values of the doped and undoped Al-Li-Zn Borate glass, derived from the mean of three measurements, are displayed in Tables 5 and 6. The repeatability of the current glass samples was calculated using Equation (10). To examine the repeatability of both doped and un-doped 1.5 mol percent Dy^{3+}, six samples of each type were subjected to 45 mGy of X-ray radiation, followed by reading, annealing, and six more rounds of radiation exposure under identical conditions. For undoped and optimally doped Al-Li-Zn Borate glass, the observed difference in the SVI value was 4% and 7.3%, respectively. The RVI or CV percent numbers show the reader's repeatability over the long term. Table 5 demonstrates that the RVI variance for Al-Li-Zn Borate, 1.5 mol percent Dy^{3+} doped and undoped, was 1.6 percent and 12.9 percent, respectively. The DVI is a metric used to quantify the TL detectors' repeatability (glass samples). Equation (10) and Table 6 define it; they display results for the high repeatability of 12.3% of the undoped sample and the reproducibility of 7.1 for 1.5 mol of Dy^{3+} doped is close to the acceptable limit of 7.5 percent (Aljewaw et al., 2023; Muhammad et al., 2019).

The repeatability of both doped and non-doped Glass Al-Li-Zn Borate was evaluated for six repeated cycles in a dose-dependent manner, as demonstrated in Figure 6 (a and b). Interestingly, with a standard deviation of less than 0.03 percent, the undoped Al-Li-Zn Borate glass sample's 4.0 percent thermoluminescence (TL) response is nearly within allowable bounds. Furthermore, the doped TL is within the permissible level by 7.1 percent. After calculation, the coefficient of variation (CV) was 7.1 percent, within the allowable range of 7.5 percent (De Carvalho et al., 2012; Mendoza-Anaya et al., 2018).

$$\text{Loss of } TL \text{ signal} = \frac{\text{Initial } TL \text{ signal} - \text{Final } TL \text{ signal}}{\text{Intial } TL \text{ signal}} \quad (11)$$

The fading of the current glass samples was evaluated with Equation (11). The TL intensity and fading features of the equivalent un-doped and optimally doped 1.5% of Dy^{3+} The glass sample of Al-Li-Zn Borate, subjected to a 45mGy x-ray radiation, as illustrated in Figures 7(a) and 8(a), correspondingly. To stop trapped electrons from escaping owing to light or temperature stimulation, the samples were stored in a black box at normal temperature. At regular intervals of 24, 48, 72, 96, 120, and 144 hours, the data were recorded. To obtain consistent readings from three samples of each data point, compre-

Table 4. The Response to 45.0 mGy X-Ray Dosages of Undoped and 1.5 mol% Dy^{3+} Doped Al-Li-Zn Borate Glass

Glass Samples	Dose Range (mGy)	Sensitivity (nC/gmGy)
Undoped Al-Li-Zn borate glass	05 – 45	2731.08
Dy^{3+} doped Al-Li-Zn borate glass	05 – 45	6527.90

Table 5. SVI Values Derived from the Mean of Three Measurements for Dy-Doped and Un-Doped LAZB Glass

	Average Number	Standard Deviation (SD)	Covariance CV= X/SD	Average Value of CV	SVI=CV×100
Undoped LAZB	0.80	0.033	0.041	0.04	4.0
	0.82	0.032	0.040		
	0.82	0.030	0.040		
Doped LAZB	25	1.6	0.064	0.073	7.3
	24.5	2.2	0.090		
	24.7	1.6	0.065		

Table 6. RVI Values Derived from Average Dy-Doped and Un-Doped Al-Li-Zn Borate Glass Measurements

Glass Samples	1st Reading	2nd Reading	3rd Reading	4th Reading	5th Reading	Mean	SD	RAVI
Undoped LAZB	1.70	1.48	1.37	1.34	1.86	1.55	0.2	12.9
Doped LAZB	36.92	36.83	36.83	35.57	35.61	36.35	0.58	1.6

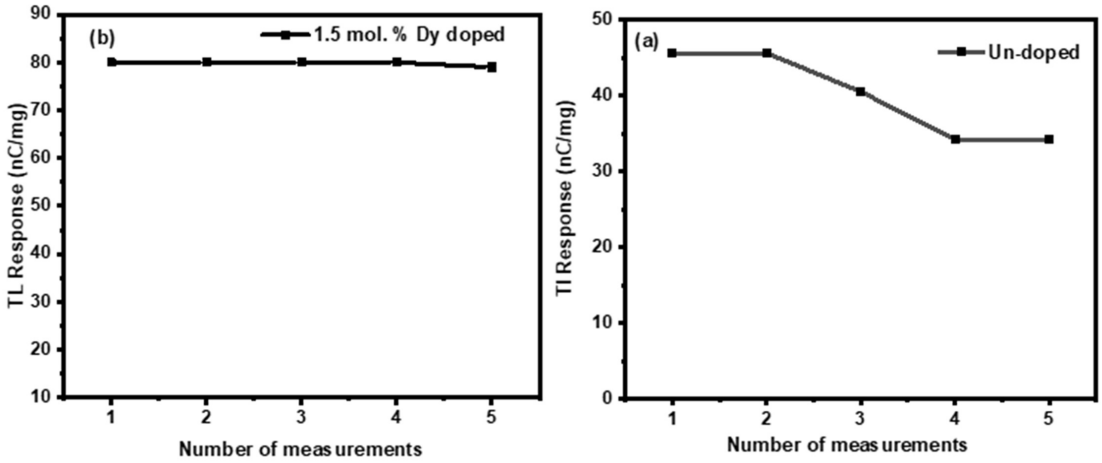

Figure 6. (a) Repeatability of Un-Doped Al-Li-Zn Borate Glass Sample (b) Consistency of Dy^{3+} Sample of Doped Al-Li-Zn Borate Glass

hensive calibration and quality assurance measurements were performed. Subsequently, for the dosimeters composed of un-doped and optimally doped 1.5 mol% of Dy^{3+}Al-Li-Zn Borate glass sample, the mean value of TL responses was calculated, with the error indicating percentage uncertainty. Twenty-four hours after irradiation, the signal for the un-doped glass was reduced by 0.84%, and for the optimally doped glass, by 0.79%. The percentage signal loss was 0.79%, 0.93%, and 0.91% after 72 hours and 0.90%, 0.91%, and 0.84% after 144 hours. These results indicated that after irradiation, the optimum doped 1.5 mol% of Dy^{3+}Al-Li-Zn Borate glass sample has dose-independent stability, showing an insignificant percentage signal loss of 0.21. According to standard and commercial dosimeters, glass dosimeters exhibit good dose linearity and low fading effects, making them valuable tools for dose measurements with low signal losses over time (Aljewaw et al., 2023; Bradley et al., 2020).

3.8 Photoluminescence (PL) Spectrum

A photoluminescence spectrum generally shows light emission peaks or bands at wavelengths, signifying changes in the electronic energy levels of the material. A photoluminescence spectrum generally shows light emission peaks or bands at wavelengths, signifying changes in the electronic energy levels

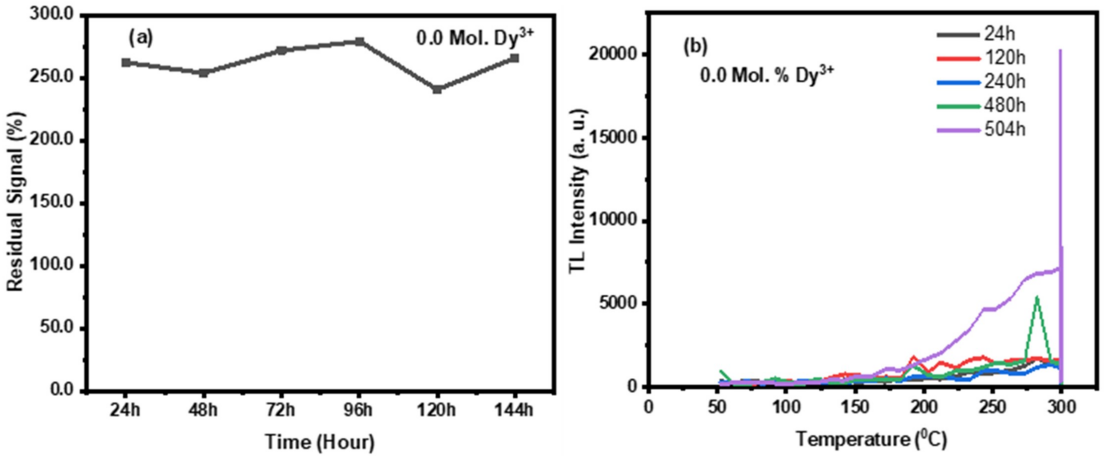

Figure 7. (a) Shows the TL Fading Response Characteristics and (b) the TL Intensity of an Un-Doped Dy^{3+} Al-Li-Zn Borate Glass Sample Exposed to a 45mGy X-Ray Dosage

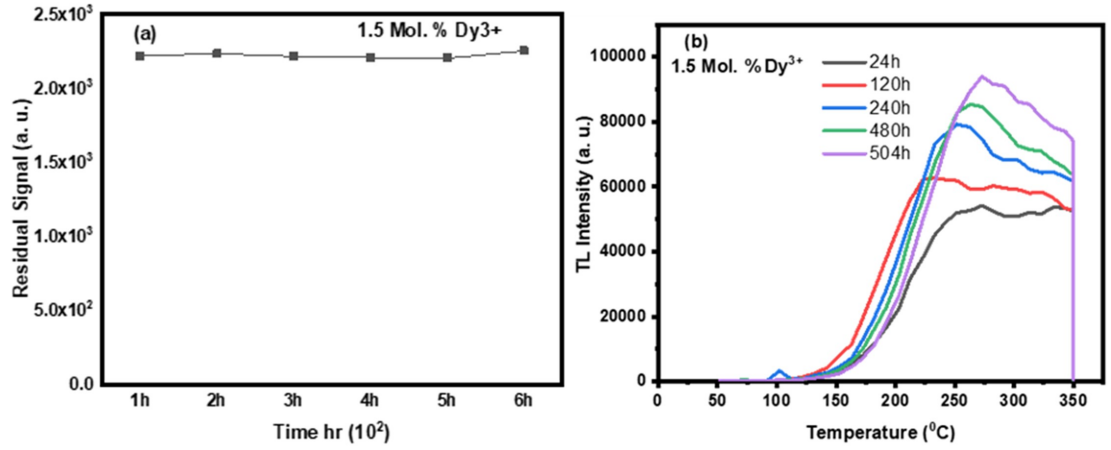

Figure 8. (a) Shows the TL Fading Response Characteristics and (b) the TL Intensity of a 1.5 Mol% Doped Dy^{3+} Al-Li-Zn Borate Glass Sample Exposed to a 45mGy X-Ray Dosage

of the material. When excited by light, these peaks' locations and intensities reveal essential details about the material's structure, composition, and behaviour. The phenomenon of PL emission in these glasses is explained by the mechanism mentioned below. The electrons are contained in the host boron ions' electron centres upon activation. The relaxation process subsequently releases the electrons, which Dy^{3+} ions then absorb. When electrons are eventually absorbed by the holes in the boron oxygen hole centre (BOHCs), also known as the recombination centre, PL is released. The PL intensity rises when Dy^{3+} is added to increase the electron sources and traps. PL spectra of the suggested Dy^{3+} doped Al-Li-Zn borate glass at 400 nm excitation are shown in Figure 9. With bright peaks at 348 nm (yellow), 529 nm (green), and 625 nm (orange hue), the composition demonstrated a good and distinct sensitivity to light which corresponded to $^4H15/2 \rightarrow {}^6P7/2$, $^4F9/2 \rightarrow {}^6H15/2$, $^4F9/2 \rightarrow {}^6H15/2$, and $^4F9/2 \rightarrow {}^6H13/2$ transitions in Dy^{3+}, respectively. (Duragkar et al., 2019; Efenji et al., 2023).

The emission photons at 348 nm and 529 nm, respectively, have yellow and blue wavelengths, which can be regarded as the hypersensitive transition in the selected rules of $\Delta L = \pm 2$: $\Delta J = \pm 2$. These are the outcomes of transitions between magnetic dipoles (MD) and electric dipoles (ED). As Figure 9 shows, this observation validates the asymmetry of the host network topology. Furthermore, this shift is consistent with the $^4H15/2 \rightarrow {}^6P7/2$ transition in Dy^{3+} ions at 348 nm (white light), which is frequently used as a reference for calibration in radiation dosimetry due to its high photoluminescence (PL) efficiency. Strongly impacting the microscopic environment of Dy^{3+} doped emission channels might impact the transition with selection rules of $\Delta L = \pm 2$; $\Delta J = \pm 2$, with intensity being highly dependent on the host. (Aljewaw et al., 2023; Hegde et al., 2019).

3.9 Minimum Detectable Dose (MDD)

The lowest amount of ionising radiation that can be detected by a detector and have a noticeable effect is referred to as the "minimum detectable dose" (MDD). It is necessary to assess its sensitivity and accuracy in detecting radiation doses. This assessment determines the lowest radiation dose level, the MDD, that the dosimeter can reliably detect (Efenji et al., 2024). Using Equation (12), the MDD values for the suggested glasses were estimated (Aljewaw et al., 2023).

$$MDD = (B* + 2\sigma_b) \times F \quad (12)$$

Where is a standard deviation, $B*$ is the dosimeter's mean background TL prior to irradiation (zero doses), and F is the calibration factor (Aljewaw et al., 2023).

The MDD values of the Al-Li-Zn borate that is undoped and Dy^{3+} doped glasses exposed to 45 mGy X-ray doses are shown in Table 7. The present glass samples' MDD was determined using empirical Equations (12). Three undoped Al-Li-Zn borate glasses and Dy^{3+} doped were annealed for the MDD measurement. The mean background signals, $B*$ were found to be 0.44 and 0.82 nC mg^{-1}. The corresponding standard deviation, σ_b , was found to be 0.04 and 0.05 nC mg^{-1}. The un-doped and Dy^{3+} doped Al-Li-Zn borate glasses have calibration factors (F) of 102 and 55 mGy $m,g^{-1}.n^{-1}$ respectively. These values were entered into Equations (12) (table 6) to obtain the mean value. The MDD values were 53.04 mGy and 45.1 mGy for the un-doped and Dy^{3+} doped Al-Li-Zn borate glasses (doped with 1.5 mol% of Dy^{3+}), respectively. As a dosimeter, it was determined that the ideal 1.5 mol% of Dy^{3+} doped and undoped Al-Li-Zn borate glasses could detect low amounts of gamma ray.

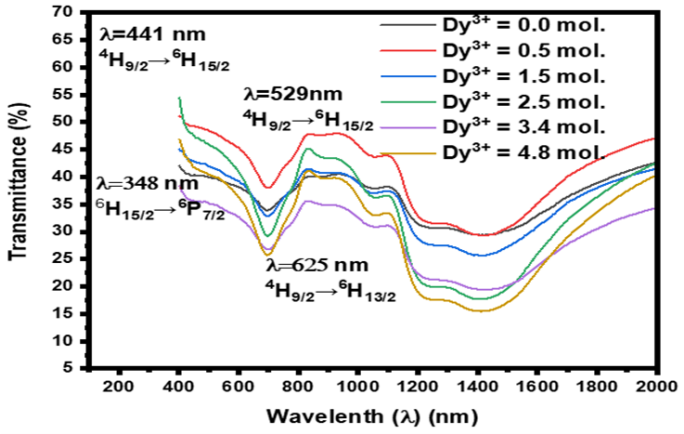

Figure 9. 45mGy X-Ray Dose Photo-Luminescence Spectrum of a 1.5% Doped Dy^{3+} Al-Li-Zn Borate Glass Sample

3.10 Effective Atomic Number ($Z_{eff.}$)

In estimating the initial dosage, tissue equivalency is a critical factor that affects the effective atomic number ($Z_{eff.}$). According to Aljewaw et al. (2023) and Bootjomchai and Laopaiboon (2014), a material is deemed "tissue equivalent" if it is $Z_{eff.}$ value is near to that of human tissue, which is 7.4 or 11.28. The evaluation was conducted using:

Table 7. MDD Values of the Un-Doped and Al-Li-Zn Borate Doped with Dy^{3+} Glasses

Glass Samples	B*	σB	F(mGymg -1nC-1)	MDD (mGy)
Undoped	0.44	0.04	102	53.04
Dy^{3+} doped	0.82	0.05	55	45.10

$$Z_{eff.} = \sqrt[3]{a_1 Z_1^m + a_2 Z_2^2 + \ldots + a_n Z_n^m} \quad (13)$$

$$a_i = \frac{n_i(Z_i)}{\Sigma_i n_i(Z_i)} \quad (14)$$

$$n_i = \left(\frac{N_A \times z_i}{A_{w.i}}.W_i\right) \quad (15)$$

Here, m is the photoelectric interaction's power dependence, which is usually adopted and equals 2.94. n_i is the amount of electrons contained in a mole, $A_{w.i}$ is the atomic weight, W_i is the fractional weight, N_A is Avogadro's number (6.02×1023 mol^{-1}), and a_i is the percentage of each element's electrons that make up the composite's overall electron content.

Equations (13), (14), and (15) were used to calculate the Zeff. value of the current glass samples. Tables 8 and 9 display the physical properties of the optimal Dy^{3+} following the Zeff. calculation, the doped Al-Li-Zn borate glass and the undoped Al-Li-Zn borate glass. Any dosimetric material's $Z_{eff.}$ value must be near biological tissues ($Z_{eff.}$ = 7.420) or bone ($Z_{eff.}$ = 11.28). The undoped Al-Li-Zn borate glass and optimal Dy^{3+} doped Al-Li-Zn borate glass was found to have $Z_{eff.}$ values of 7.30 and 9.3, which are human tissues and near-bones values, respectively (Bootjomchai and Laopaiboon, 2014).

The $Z_{eff.}$ value of 7.30 in undoped glass represents the effective nuclear charge that an electron experiences in the material, which influences the material's interaction with radiation. Stronger interactions, which affect the material's reaction to radiation, are indicated by a more considerable $Z_{eff.}$ value. Doping glass with Dy3+ ions raises the $Z_{eff.}$ to 9.3, improving the material's capacity to absorb and react to radiation. Its higher Z value indicates better radiation sensitivity, which increases its effectiveness as a radiation dosimetric material (Aljewaw et al., 2023; Rivera, 2012).

3.11 Differential Thermal Analysis (DTA)

The stability of its glass network is determined by the transition temperature (T_g) and crystallisation temperature (T_c), which both indicate the glass-forming ability (GFA). High GFA and strength are typically found in materials with low T_c and high T_g. On the other hand, the stability and glass-forming ability (GFA) of materials with low and high Tg are inferior. As shown

Table 8. Characteristics of the Undoped Al-Li-Zn Borate Glass Dosimeter for $Z^{eff.}$ Analysis

	$A_{w.i}(g)$	Z_i	W_i	a_i	$\frac{(N_A \times Z_i \times W_i)}{A_{w.i}}$	$a \times Z$	$Z^{2.94}$	$a.Z^{2.94}$
Al	26.98	13	1.153	0.012	0.56	0.48	1883.62	22.30
Zn	65.98	30	1.371	0.013	0.62	0.45	22015.90	292.46
B	10.81	5	2.137	0.021	0.99	0.46	113.49	2.39
O	16	8	5.339	0.057	2.67	0.50	451.94	25.71
Total					4.84			342.86
$Z_{eff.}$								7.30

Table 9. Characteristics of the Dy^{3+} Infused Al-Li-Zn Borate Glass Dosimeter for $Z^{eff.}$ Analysis

	$A_{w.i}(g)$	Z_i	W_i	a_i	$\frac{(N_A \times Z_i \times W_i)}{A_{w.i}}$	$a \times Z$	$Z^{2.94}$	$a.Z^{2.94}$
A	26.98	13	1.310	0.077	0.310	0.41	1883.6	21.66
Zn	65.98	30	1.575	0.016	0.759	0.48	22015.9	662.92
B	10.81	5	1.607	0.016	0.731	0.45	113.5	0.59
O	16	8	5.354	0.053	2.476	0.46	451.9	13.57
Dy	162.5	66	0.153	0.001	0.077	0.50	223593.4	
Total					4.042			698.73
$Z_{eff.}$								9.3

Table 10. The Values of T_g, T_c, and T_m Were Undoped and 1.5 mol Dy^{3+} Doped Al-Li-Zn Borate Glass

Parameters	Undoped Sample	1.5 mol Dy^{3+} Doped
T_g	257	101
T_c	756	444
T_m	862	815

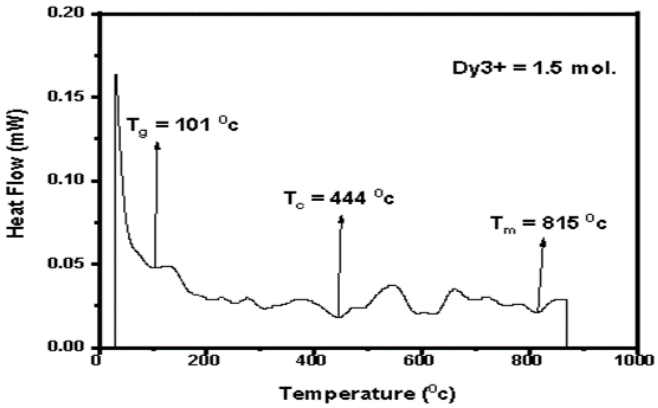

Figure 10. Differential Thermal Study of the Undoped Al-Li-Zn Borate Glass

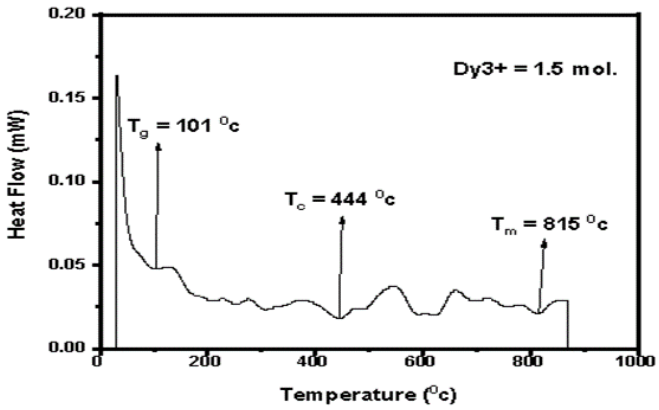

Figure 11. Differential Thermal Analysis of 1.5 mol Dy^{3+} Doped Al-Li-Zn Borate Glass

in Table 10, Equations (16) and (17) were used to determine the materials' glass-forming ability (GFA) and glass stability (GS).

$$GFA = \frac{T_c - T_g}{T_m - T_g} \tag{16}$$

$$GS = \frac{(T_c - T_g)}{T_g} \tag{17}$$

The values for the three parameters T_g, T_c, and T_m undoped and at 0.5 mol are given in Table 9, Figures 10 and 11. Al-Li-Zn borate glass doped with Dy^{3+}. The symbols T_g, T_m, and T_z stand for the glass transition, crystallisation, and melting temperatures, respectively, of the material. Due to their potential to affect the material's luminescence qualities, these parameters are relevant to thermoluminescence investigations. For example, Tg indicates the energy required to activate the

material's luminous centres. Likewise, T_c affects the motion of the flaws that provide the luminescence signal when heated (Jaidass et al., 2018). The ideal T_g value would guarantee the material's thermal stability and be low enough to allow for the effective migration of flaws during heating. Depending on the study's objectives, T_m can also be pertinent (Ezra et al., 2024; El-Faramawy et al., 2021).

The doped material transitions towards a more flexible and rubbery state at lower temperatures, as seen by the considerable T_g dropped in the doped sample from 101°C to 257°C in the undoped sample. The radiation sensitivity of the material and its capacity to precisely record radiation doses may be impacted by this modification (Razak et al., 2016). Reduced T_g values might improve the material's radiation sensitivity, making it better suited for TLD applications. The doped samples T_c decreased from 756°C to 444°C, indicating a lower temperature at which crystallisation starts (Bradley et al., 2020). This alteration may impact the material's dosimetric capabilities by changing its structural characteristics and electron-trapping capacity. A lower T_c indicates increased radiation sensitivity and better dosimetric performance in TLDs. The doped samples T_m decreased somewhat from 862°C to 815°C, indicating a lower transition temperature for the material from a solid to a liquid state. The material's stability and reaction to radiation exposure may be affected by this modification. A lower Tm might make the material better suited for TLD applications by improving its capacity to hold onto radiation-induced signals (Furetta et al., 2001).

3.12 Fourier Transform Infrared Spectroscopy (FTIR)

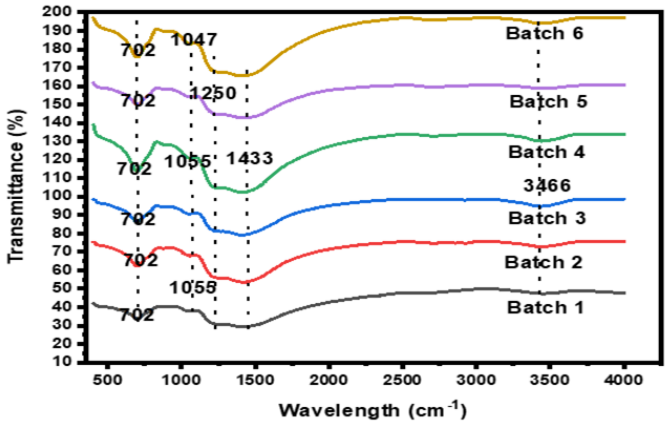

Figure 12. FTIR Spectra of Dy^{3+} Doped and Undoped Al-Li-Zn Borate Glasses with Different Composition

The glass's functional groups were bonded together, as seen in Figure 12, by means of FTIR spectroscopy (Perkin Elmer, USA). With a resolution of 0.85 cm^{-1}, the FTIR provides spectra in the thin pellet method that span 400–4000 cm^{-1} at a pressure of 77.2 MP. To cut down on inaccuracies, the average of the standard pellets is displayed in each infrared spectrum. Four components of the borate are visible in the infrared transmittance spectra of the glasses, as shown in Figure 12: clusters of BO_4, BO_3 groups, and OH groups, in addition to B–O–B vibrations. These were broad, weak, medium-sized, and considerable peaks.

Important chemical structures and functional groups are seen in the FT-IR spectra of Al-Li-Zn borate glass activated by Dy^+ ions. In line with the reported work of Ullah et al. (2024), the peak at 702 cm^{-1}, which could be a representation of boroxol rings or borate structures, indicates B−O−B bending vibrations. The absorption at 1047 cm^{-1} reflects the asymmetric stretching of B−O bonds in BO_4 units, which is suggestive of tetrahedral boron. The band located at 1250 cm^{-1}, which is associated with B−O stretching in BO_3 units, represents trigonal borate groups. The presence of hydroxyl groups in the glass network was suggested by the B−O−H bending vibrations displayed by the 1433 cm^{-1} peak. Our results, in agreement with earlier studies, validate the complex borate network with tetrahedral and trigonal boron environments and tiny hydroxyl impurities, which are essential for characterising the glass for radiation dosimetry applications (Abdou et al., 2020; Ullah et al., 2024).

4. CONCLUSIONS

This study and investigation results highlight the tissue-equivalent thermoluminescent glass detector based on Al-Li-Zn borate oxide doped with Dy^{3+}, which shows promising features and dosimetric performances. Its tissues' equivalent effective atomic number ($Z_{eff.}$) value was increased from 7.30 to 9.3 after doping the glass with Dy^{3+} ions, enhancing its radiation sensitivity and capacity to absorb and react to radiation. The material is a good choice for precise and trustworthy radiation dosimetry because of its amorphous structure, stability, structural capacity, and particle size dispersion, which were verified with XRD examination, FTIR, and FESEM. The glass samples' FTIR analysis indicates four parts of the borate, namely: B–O–B vibrations, clusters of BO_4, BO_3 groups, and OH groups. These peaks were substantial, medium, weak, and broad. The measured bandgap values suggest the possibility of effective energy absorption and thermoluminescent emission. The 1.5 mol% Dy^{3+} doped glass showed a 3796 nC/mgGy times higher TL sensitivity than the un-doped glass with the reproducibility of 12.3% of the undoped sample and high reproducibility of 7.1 for 0.10 mol of Dy^{3+} doped, which is close to the acceptable limit of 7.5. The sample shows a fading reduction of 0.84% for the undoped and 0.79% for the 1.5 moles doped glass 24 hours after irradiation. The percentage signal loss was 0.79%, 0.93%, and 0.91% after 72 hours and 0.90%, 0.91%, and 0.84% after 144 hours. The MDD values were 53.04 mGy and 45.1 mGy for the un-doped and 1.5 moles Dy^{3+} doped Al-Li-Zn borate glasses, respectively. The bright peaks in the PL spectra were located at 348 nm (yellow), 529 nm (green), and 625 nm (orange hue), corresponding to the $^4H15/2 \rightarrow {}^6P7/2$, $^4F9/2 \rightarrow {}^6H15/2$, $^4F9/2 \rightarrow {}^6H15/2$, and $^4F9/2 \rightarrow {}^6H13/2$ transitions in Dy^{3+}, respectively. The frequency factor and activation energy of the 1.5 mol Dy^{3+} doped Al-Li-Zn borate are 2.1×10

27 s^{-1} and 1.03 eV, respectively. Future research endeavours might concentrate on refining the glass's composition and reaction to various radiation intensities to improve its dosimetric performance further and increase its usability in all areas of radiation dosimetry applications.

5. ACKNOWLEDGMENT

We appreciate the research facilities provided by Universiti Sains Malaysia, USM Short Term Grant Q (account number 304.CSERC.6315568). We also thank Federal University Lokoja in Nigeria for its sponsorship and financial support. We especially want to thank our supervisor, Assoc. Professor Dr. Iskandar Shahrim Mustafa.

REFERENCES

Abdou, N. Y., M. M. Farag, and W. M. Abd-Allah (2020). Thermoluminescent Properties of Nano-Magnesium Phosphate Ceramic for Radiation Dosimetry. *European Physical Journal Plus*, **135**(3); 317

Aljewaw, O. B., M. K. A. Karim, N. Effendy, H. M. Kamari, M. H. M. Zaid, N. M. Noor, A. A. Salim, N. M. Isa, A. B. A. Kadir, M. T. Chew, and A. I. Abokridiga (2023). Physical, Optical and Thermoluminescence Properties of Lithium Aluminum Borate Glass Co-Doped with Dy_2O_3. *Radiation Physics and Chemistry*, **209**; 111004

Aljewaw, O. B., M. K. A. Karim, H. M. Kamari, M. H. M. Zaid, N. M. Noor, I. N. C. Isa, and M. H. A. Mhareb (2020). Impact of Dy_2O_3 Substitution on the Physical, Structural and Optical Properties of Lithium–Aluminium–Borate Glass System. *Applied Sciences (Switzerland)*, **10**(22); 1–17

Aydas, C., U. R. Yüce, B. Engin, and G. S. Polymeris (2016). Dosimetric and Kinetic Characteristics of Watch Glass Sample. *Radiation Measurements*, **85**; 78–87

Bootjomchai, C. and R. Laopaiboon (2014). Thermoluminescence Dosimetric Properties and Effective Atomic Numbers of Window Glass. *Nuclear Instruments and Methods in Physics Research, Section B: Beam Interactions with Materials and Atoms*, **323**; 42–48

Bradley, D. A., M. U. Khandaker, and A. Alanazi (2020). Irradiated Glass and Thermoluminescence Yield: Dosimetric Utility Reviewed. *Radiation Physics and Chemistry*, **170**; 108680

Chen, R. (1969). On the Calculation of Activation Energies and Frequency Factors from Glow Curves. *Journal of Applied Physics*, **40**(2); 570–585

Chen, R. and S. A. A. W. (1970). Effects of Various Heating Rates on Glow Curves. *Journal of Applied Physics*, **41**(13); 5227–5232

De Carvalho, A. B., T. F. Barros, P. L. Guzzo, and H. J. Khoury (2012). Manufacturing Polycrystalline Pellets of Natural Quartz for Applications in Thermoluminescence Dosimetry. *Materials Research*, **15**(4); 536–543

Duragkar, A., A. Muley, N. R. Pawar, V. Chopra, N. S. Dhoble, O. P. Chimankar, and S. J. Dhoble (2019). Versatility of Thermoluminescence Materials and Radiation Dosimetry – A Review. *Luminescence*, **34**(7); 656–665

Efenji, G. I., S. M. Iskandar, N. N. Yusof, J. A. Rabba, O. I. Mustapha, I. M. Fadhirul, S. A. Umar, et al. (2024). Structural Properties of Thermoluminescence Dosimeter Materials, Preparation, Application, and Adaptability: A Systematic Review. *Journal of Applied Sciences and Environmental Management*, **28**(4); 1129–1150

Efenji, G. I., I. S. Mustafa, F. A. Kamgba, O. O. Ogunleye, T. H. Khazaalah, N. S. Ezra, H. S. Naeem, H. M. Shariff, M. Jamil, and M. F. I. Abdul Malik (2023). Description and Dosimetric Features of Lithium Borate Glass Doped with Transition Metals for Thermoluminesce, a Re-Evaluation. *Physica Scripta*, **98**(5)

El-Adawy, A., N. E. Khaled, A. R. El-Sersy, A. Hussein, and H. Donya (2010). TL Dosimetric Properties of Li_2O-B_2O_3 Glasses for Gamma Dosimetry. *Applied Radiation and Isotopes*, **68**(6); 1132–1136

El-Faramawy, N., A. El-Naggar, C. Woda, and M. El-Kinawy (2021). Investigation of TL Dosimetric Parameters of Lithium Borate Glass Doped with Dysprosium. *Optical Materials*, **113**; 110672

Ezra, N. S., I. S. Mustafa, M. Sayyed, K. Dakok, I. Fadhirul, T. H. Khazaalah, G. Efenji, M. Jamil, H. S. Naeem, A. Oke, and A. S. A. Idriss (2024). Synthesis, and Impact of GaN Deposition on the Physical, Optical, and Structural Properties of Nd^{3+}-Doped Na_2O Borate Glasses Prepared with Soda Lime (SLS) Glass as a Silica Source. *Optical Materials*; 115907

Furetta, C., M. Prokic, R. Salamon, and R. Prokic (2001). Dosimetric Characteristics of Tissue Equivalent Thermoluminescent Solid TL Detectors Based on Lithium Borate. *Nuclear Instruments Methods Phys Res A*, **456**; 411–417. N.d.

Godwin, E., S. M. Iskandar, K. Ferdinand, K. Ogunleye, T. Khazaalah, H. Salah Naeem, N. S. Ezra, M. F. I. Abdul Malik, M. Jamil, and H. M. Shariff (2023). Description and Dosimetric Features of Lithium Borate Glass Doped with Transition Metals for Thermoluminesce, a Re-Evaluation. *Physica Scripta*, **98**; August 2022

Hashim, S., M. H. A. Mhareb, S. K. Ghoshal, Y. S. M. Alajerami, M. I. Saripan, and D. A. Bradley (2017). Luminescence Features of Dysprosium and Phosphorus Oxide Co-Doped Lithium Magnesium Borate Glass. *Radiation Physics and Chemistry*, **137**; 45–48

Hegde, V., N. Chauhan, C. S. D. Viswanath, V. Kumar, K. K. Mahato, R. Buwane, and S. J. Dhoble (2019). Photoemission and Thermoluminescence Characteristics of Dy^{3+} -Doped Zinc Sodium Bismuth Borate Glasses. *Journal of Luminescence*, **209**; 337–343

Jaidass, N., C. K. Moorthi, A. M. Babu, and M. R. Babu (2018). Luminescence Properties of Dy^{3+} Doped Lithium Zinc Borosilicate Glasses for Photonic Applications. *Heliyon*, **4**(3); e00555

Jamil, M., I. S. Mustafa, N. M. Ahmed, S. B. S. Hamid, T. H. Khazaalah, E. Godwin, N. S. Ezra, and H. N. Salah (2023).

Poly (Ethylene) Oxide/Erbium Oxide as T2 and T1-T2 Dual-Mode MRI Diagnostic Nanofibres. *Ceramics International*, **49**(13); 22429–22439

Khandaker, M. U., A. Taheri, and D. A. Bradley (2024). A Systematic Review on the Silica Fibre Thermoluminescence Dosimeters for Medical Applications. *Journal of Radioanalytical and Nuclear Chemistry*, **333**(3); 1507–1530

Khazaalah, T. H., I. Shahrim Mustafa, H. Al-Ghamdi, A. Abdul Rahman, M. Sayyed, A. H. Almuqrin, M. H. Mohd Zaid, R. Hisam, M. F. I. Abdul Malik, N. Seth Ezra, et al. (2022). The Effect of WO_3-Doped Soda Lime Silica SLS Waste Glass to Develop Lead-Free Glass As a Shielding Material against Radiation. *Sustainability*, **14**(4); 2413

Mendoza-Anaya, D., A. González-Romero, O. Ávila, P. R. González, and L. Escobar-Alarcón (2018). Thermally Stimulated Luminescence of $Li_2B_4O_7$:Cu, Ag, P+PTFE. *Journal of Luminescence*, **204**; 176–181

Mhareb, M. H. A., S. Hashim, S. K. Ghoshal, Y. S. M. Alajerami, M. J. Bqoor, A. I. Hamdan, M. A. Saleh, and M. K. B. A. Karim (2016). Effect of Dy_2O_3 Impurities on the Physical, Optical and Thermoluminescence Properties of Lithium Borate Glass. *Journal of Luminescence*, **177**; 366–372

Morsi, R. M. M., S. Ibrahim, S. Abo-Naf, and M. M. Morsi (2016). Effect of Alkaline Earth Metal Oxides on the Dielectric, Structural and Physico-Chemical Properties of Lithium–Zinc–Lead-Borates. *Journal of Materials Science: Materials in Electronics*, **27**(4); 4147–4156

Muhammad, N. A., M. K. A. Karim, H. A. Hassan, M. A. Kamarudin, J. H. D. Wong, and M. J. Ibahim (2019). Estimation of Effective Dose and Organ Cancer Risk from Paediatric Computed Tomography Thorax–Abdomen–Pelvis Examinations. *Radiation Physics and Chemistry*, **165**; 108438

Pal, M., B. Roy, and M. Pal (2011). Structural Characterisation of Borate Glasses Containing Zinc and Manganese Oxides. *Journal of Modern Physics*, **02**(09); 1062–1066

Pawar, P. P., S. R. Munishwar, and R. S. Gedam (2017). Intense White Light Luminescent Dy3+ Doped Lithium Borate Glasses for W-LED: A Correlation Between Physical, Thermal, Structural and Optical Properties. *Solid State Sciences*, **64**; 41–50

Pekpak, E., O. Gülhan, and Y. Aysen (2009). Thermoluminescent Characteristics of Lithium Tetraborate. In *IV International Boron Symposium*. Eskişehir, Turkey, pages 15–17

Pekpak, E., A. Yilmaz, and G. Ozbayoglu (2014). An Overview on Preparation and TL Characterization of Lithium Borates for Dosimetric Use. *The Open Mineral Processing Journal*, **3**(1); 14–24

Pekpak, E., A. Yilmaz, and G. Özbayolu (2011). The Effect of Synthesis and Doping Procedures on Thermoluminescent Response of Lithium Tetraborate. *Journal of Alloys and Compounds*, **509**(5); 2466–2472

Prabhu, N. S., V. Hegde, A. Wagh, M. I. Sayyed, O. Agar, and S. D. Kamath (2019). Physical, Structural and Optical Properties of Sm^{3+} Doped Lithium Zinc Alumino Borate Glasses. *Journal of Non-Crystalline Solids*, **515**; 116–124

Prabhu, N. S., K. Sharmila, S. Kumaraswamy, H. M. Somashekarappa, M. I. Sayyed, H. Al-Ghamdi, A. H. Almuqrin, and S. D. Kamath (2021). An Examination of the Radiation-Induced Defects and Thermoluminescence Characteristics of Sm_2O_3 Doped BaO-ZnO-LiF-B_2O_3 Glass System for γ-Dosimetry Application. *Optical Materials*, **118**; 111252

Razak, N. A., S. Hashim, M. H. A. Mhareb, and N. Tamchek (2016). Photoluminescence and Thermoluminescence Properties of Li_2O-Na_2O-B_2O_3 Glass. *In Luminescence*, **31**(3); 754–759

Rivera, T. (2012). Thermoluminescence in Medical Dosimetry. *Applied Radiation and Isotopes*, **71**(SUPPL.); 30–34

Saidu, A., H. Wagiran, M. Saeed, and Y. Alajerami (2014). Structural Properties of Zinc Lithium Borate Glass. *Optics and Spectroscopy*, **117**; 396–400

Saidu, A., H. Wagiran, M. A. Saeed, and Y. S. M. Alajerami (2015). Thermoluminescence Characteristics of Zinc Lithium Borate Glass Activated with Cu^+ (ZnO-Li_2O-B_2O_3:Cu^+) for Radiation Dosimetry. *Journal of Radioanalytical and Nuclear Chemistry*, **304**(2); 627–632

Saidu, A., H. Wagiran, M. A. Saeed, H. K. Obayes, A. Bala, and F. Usman (2018). Thermoluminescence Response of Rare Earth Activated Zinc Lithium Borate Glass. *Radiation Physics and Chemistry*, **144**; 413–418

Sani, S. F. A., M. H. U. Othman, A. Alqahtani, K. S. Almugren, F. H. Alkallas, and D. A. Bradley (2020). Low-Cost Commercial Borosilicate Glass Slides for Passive Radiation Dosimetry. *PLoS ONE*, **15**(12 December); 1–16

Satkar, R. C., A. R. Kadam, D. A. Ovhal, and S. Dhoble (2021). Inorganic Thermoluminescent Phosphors in Radiation Dosimetry: An Overview. In *Journal of Physics: Conference Series*, volume 1913. IOP Publishing, page 012023

Shafaei, M. A. and S. Moradi (2023). Production of Thermoluminescent Dosimetry (TLD) Chip from LiF Powder Using Thermal Process Method and Comparing Energy and Density of its Traps with TLD100. *International Journal of Applied Physics*, **10**(2); 7–15

Stanković Petrović, J. S., Z. I. Knežević, N. L. Krźanović, M. C. Majer, M. Z. Živanović, and O. F. Ciraj-Bjelac (2021). Review of the Thermoluminescent Dosimetry Method for the Environmental Dose Monitoring. *Nuclear Technology and Radiation Protection*, **36**(2); 150–162

Ullah, B., M. B. Kakakhel, S. Ur Rehman, M. T. Siddique, M. Munir, K. Ahmad, M. M. Mahmood, M. Wazir-ud Din, and I. Anjum (2024). Synthesis and Dosimetric Characterisation of Lithium Tetraborate ($Li_2B_4O_7$:Cu,Ag) Thermoluminescent Dosimeter with Improved Reproducibility and Reusability. *Radiation Physics and Chemistry*, **220**; 111704

Wahib, N. B., M. U. Khandaker, S. F. Abdul Sani, K. S. Al-Mugren, D. A. Bradley, A. Sulieman, M. R. I. Faruque, and M. I. Sayyed (2020). The Potential Use of Car Windscreens for Post-Accident Dose Reconstruction in the Periphery of Nuclear Installations. *Applied Sciences (Switzerland)*, **10**(20);

1–14
White, A. J., S. P. Jollota, C. G. Hammer, A. U. Khan, L. A. DeWerd, and W. S. Culberson (2024). Thermoluminescent Dosimeters (TLD-100) for Absorbed Dose Measurements in Alpha-Emitting Radionuclides. *Applied Radiation and Isotopes*, **208**; 111307